



Dynamics of a Rydberg hydrogen atom near a metal surface in the electron-extraction scheme



Manuel Iñarrea^a, Víctor Lanchares^b, Jesús Palacián^c, Ana I. Pascual^b,
J. Pablo Salas^{a,*}, Patricia Yanguas^c

^a Área de Física Aplicada, Universidad de La Rioja, Logroño, Spain

^b Departamento de Matemáticas y Computación, Universidad de La Rioja, Logroño, La Rioja, Spain

^c Departamento de Ingeniería Matemática e Informática, Universidad Pública de Navarra, Pamplona, Spain

ARTICLE INFO

Article history:

Received 20 August 2014
Received in revised form 27 October 2014
Accepted 3 November 2014
Available online 13 November 2014
Communicated by A.P. Fordy

Keywords:

Interactions of atoms with surfaces
Nonlinear Hamiltonian dynamics
Charge transfer

ABSTRACT

We study the classical dynamics of a Rydberg hydrogen atom near a metal surface in the presence of a constant electric field in the electron-extraction situation [1], e.g., when the field attracts the electron to the vacuum. From a dynamical point of view, this field configuration provides a dynamics richer than in the usual ion-extraction scheme, because, depending on the values of field and the atom–surface distance, the atom can be ionized only towards the metal surface, only to the vacuum or to the both sides. The evolution of the phase space structure as a function of the atom–surface distance is explored in the bound regime of the atom. In the high energy regime, the ionization mechanism is also investigated. We find that the classical results of this work are in good agreement with the results obtained in the wave-packet propagation study carried out by So et al. [1].

© 2014 Elsevier B.V. All rights reserved.

1. Introduction

In the study of charge transfer processes between a Rydberg atom and a metal surface, an electric field perpendicular to the metal surface in the ion-extraction scheme is usually applied [2]. Under this scheme, and after the electron is captured by the surface, the Coulomb force on the positive ion neutralizes the metal attraction and the ion escapes the surface providing useful information on the atom–surface ionization distance. The reversed ion-extraction field situation was considered by So et al. [1] for a Rydberg hydrogen atom. The wave packet propagation study of the ionization of the system performed by these authors resulted in significant differences between the “normal” and the reversed situations. From a classical point of view, a comprehensive study of the dynamics of this system in the ion-extraction scheme was done in [3]. Following the same classical approach, the aim of this paper is to study the interaction of a Rydberg hydrogen atom with a metal surface in the presence of an electric field in the electron-extraction scheme.

The structure of the paper is organized as follows. In Section 2, the classical Hamiltonian of the system is presented, and the main features of the real potential are described. Section 3 is devoted to

the study of the dynamics of the Rydberg electron in the bound regime, that is, for low energy system values. Section 4 is focussed on the dynamics of the system in the unbound regime for high enough energy values, where the ionization of the atom is possible. Finally, conclusions are presented in Section 5. Atomic units are used throughout the paper.

2. The problem: Rydberg hydrogen atom near a metal surface

We consider the motion of an electron in a Coulomb field induced by a infinitely massive nucleus of charge $e > 0$ at the origin of the coordinate system. The metal surface is located at the plane $z = -d$, and a constant electric field of strength f along the z -axis is superimposed. In cylindrical coordinates $(\rho, z, \phi, P_\rho, P_z, P_\phi)$ and atomic units, the Hamiltonian \mathcal{H} of the system reads

$$\mathcal{H} = \frac{P_\rho^2 + P_z^2}{2} + \frac{P_\phi^2}{2\rho^2} - \frac{1}{r} + fz + \frac{1}{\sqrt{\rho^2 + (2d+z)^2}} - \frac{1}{4(d+z)}, \quad (1)$$

where $r = \sqrt{\rho^2 + z^2}$. The last two terms in \mathcal{H} account for the image model describing the interaction of the atom with the surface [4]. Owing to the axial symmetry, the z component P_ϕ of the angular momentum is conserved and (1) defines a two-degree-of-freedom dynamical system. We consider in this paper the case

* Corresponding author.

E-mail address: josepablo.salas@unirioja.es (J.P. Salas).

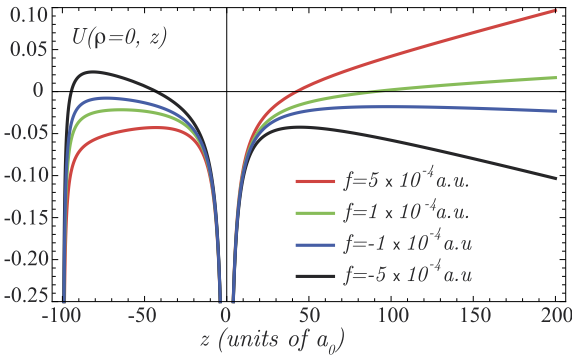


Fig. 1. Effective potential curves $U(\rho=0, z)$ for several values of the electric field f . The atom–surface distance is fixed at $d = 100a_0$.

$P_\phi = 0$ in such a way that, besides the energy $E = \mathcal{H}$, the system will depend on the external parameters d and f . The equations of motion of Hamiltonian (1) are

$$\begin{aligned} \dot{\rho} &= P_\rho, & \dot{z} &= P_z, \\ \dot{P}_\rho &= \frac{\rho}{((2d+z)^2 + \rho^2)^{3/2}} - \frac{\rho}{(\rho^2 + z^2)^{3/2}}, \\ \dot{P}_z &= \frac{2d+z}{((2d+z)^2 + \rho^2)^{3/2}} - \frac{1}{4(d+z)^2} - f - \frac{z}{(\rho^2 + z^2)^{3/2}}. \end{aligned} \quad (2)$$

In Hamiltonian (1) we can define the effective potential $U(\rho, z)$

$$U(\rho, z) = -\frac{1}{r} + fz + \frac{1}{\sqrt{\rho^2 + (2d+z)^2}} - \frac{1}{4(d+z)}, \quad (3)$$

which presents a singularity at the origin. For $f > 0$ (ion-extraction scheme), $U(\rho, z)$ has a unique critical point (see [3] and references therein). More precisely, it is a saddle point $(\rho, z) = (0, z_n)$ located at the negative side of the z -axis. This is the potential barrier that the electron overcomes when it is captured by the metal surface. For $f > 0$, the escape of the electron to the vacuum side is forbidden. The potential curves $U(\rho=0, z)$ for $f = 5 \times 10^{-4}$ a.u. and for $f = 1 \times 10^{-4}$ a.u. in Fig. 1 illustrate this case. However, when the electric field is negative, $f < 0$ (electron-extraction scheme), $U(\rho, z)$ presents an additional saddle point $(\rho, z) = (0, z_p)$ at the positive part of the z -axis. Through this new potential barrier, the electric field can drag the electron to the vacuum side. This case is depicted in Fig. 1 for $f = -5 \times 10^{-4}$ a.u. and for $f = -1 \times 10^{-4}$ a.u. The electron capture by the surface is enhanced with increasing positive electric field values because the surface potential barrier becomes lower. However, decreasing negative electric field values obstruct the surface ionization process (increasingly higher surface barrier), while the vacuum ionization process is enhanced (decreasingly lower vacuum barrier). Because in this study we consider negative electric field values, in Fig. 2 it is shown a detailed evolution of the position, z_p and z_n , and the energies, E_{z_p} and E_{z_n} , of the saddle points as a function of the distance d .

The usual way to avoid the numerical problems involved with the Coulomb singularity is to apply the well known Levi-Civita regularization [5]. This procedure starts with a change to semi-parabolic coordinates (u, v) ,

$$\rho = uv, \quad z = (u^2 - v^2)/2, \quad (4)$$

$$u = \pm\sqrt{r+z}, \quad v = \pm\sqrt{r-z}. \quad (5)$$

Next, we define a new scaled time $\tau = t/(u^2 + v^2)$. Finally, after an overall multiplication by $u^2 + v^2$, the Hamiltonian (1) reads

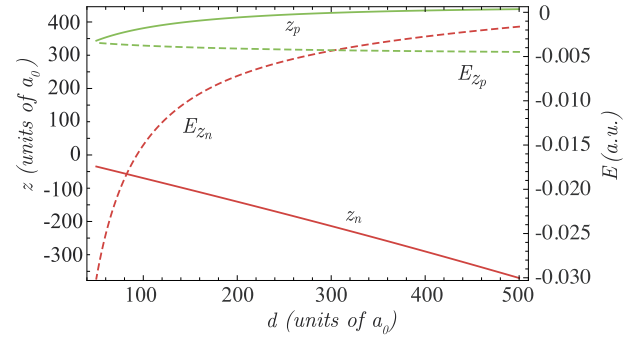


Fig. 2. Position (solid lines) and energy (dashed lines) of the saddle points $(0, z_n)$ and $(0, z_p)$ for $f = -5 \times 10^{-6}$ a.u. and for varying distance d .

$$\begin{aligned} \mathcal{K} &= 2 \\ &= \frac{P_u^2 + P_v^2}{2} - E(u^2 + v^2) + \frac{f}{2}(u^4 - v^4) \\ &\quad + \frac{2(u^2 + v^2)}{\sqrt{4du^2v^2 + (4 + u^2 - v^2)^2}} - \frac{u^2 + v^2}{2(2d + u^2 - v^2)}, \end{aligned} \quad (6)$$

where

$$P_\rho = \frac{vP_u + uP_v}{u^2 + v^2}, \quad P_z = \frac{uP_u - vP_v}{u^2 + v^2}, \quad (7)$$

$$P_u = vP_\rho + uP_z, \quad P_v = uP_\rho - vP_z. \quad (8)$$

Thence, the regularized Hamiltonian (6) enables to study the dynamics of orbits that, at a given moment, collide with the nucleus. Note that the regularized Hamiltonian \mathcal{K} takes a constant value 2 and that the energy E appears as a parameter in \mathcal{K} . The regularized equations of motion of Hamiltonian (6) are given by

$$\begin{aligned} \dot{u} &= P_u, & \dot{v} &= P_v, \\ \dot{P}_u &= -\frac{\partial \mathcal{K}}{\partial u}, & \dot{P}_v &= -\frac{\partial \mathcal{K}}{\partial v}. \end{aligned} \quad (9)$$

Rectilinear trajectories are typical colliding orbits. It is easy to check that rectilinear orbits along the z -axis are particular solutions in the equations of motion (2). These rectilinear orbits are a convenient example of how the described regularization procedure works. In Fig. 3 is shown the time evolution of two rectilinear trajectories for $d = 100$ a.u. and for $f = -5 \times 10^{-6}$ a.u. along the z -axis with initial conditions $(\rho, P_\rho, z, P_z) = (0, 0, 45.1861, 0)$ and $(\rho, P_\rho, z, P_z) = (0, 0, -45.2000, 0)$, e.g., at the positive and at the negative part of the z -axis, respectively. These initial conditions were previously converted to regularized coordinates using (4)–(8) and they were numerically propagated by using the regularized equations of motion (9). As we observe in that figure, the trajectory with positive (negative) z initial condition is always moving in the positive (negative) z -axis because, when the electron collides with the nucleus, it bounces back. In other words, we have two different families of rectilinear periodic orbits along the z -axis which are kept apart by the Coulomb singularity. For historical reasons, we name these rectilinear families as I_∞^+ ($z \geq 0$) and I_∞^- ($z \leq 0$), respectively.

3. Phase space structure

It is well known that the phase space is mainly characterized by the number and stability of the periodic orbits existing in phase space [6]. For two-degree-of-freedom Hamiltonian systems, Poincaré surfaces of section are a useful tool to uncover the phase space structure. In our problem, the surface of section is defined as the intersection of the phase trajectories with the $\rho = 0$ plane with $P_\rho \geq 0$. Thus, the surfaces of section lie in the (z, P_z) plane limited by the curves

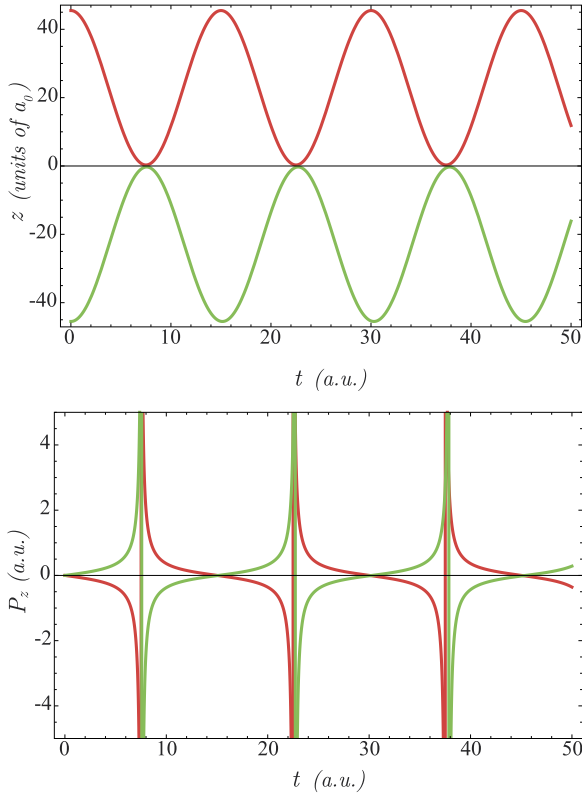


Fig. 3. Rectilinear orbits along the z -axis. Red lines correspond to an orbit with initial conditions $(\rho, P_\rho, z, P_z) = (0, 0, 45.1861, 0)$, while green lines correspond to an orbit with initial conditions $(\rho, P_\rho, z, P_z) = (0, 0, -45.2000, 0)$. Both orbits for $d = 100a_0$, $f = -5 \times 10^{-6}$ a.u. and energy $E = -0.02$ a.u. (For interpretation of the references to color in this figure legend, the reader is referred to the web version of this article.)

$$P_z = \pm \sqrt{2 \left(\frac{1}{4(d+z)} - \frac{1}{2d+z} + E - fz + \frac{1}{|z|} \right)}. \quad (10)$$

Note that the rectilinear orbits I_∞^+ and I_∞^- are tangent to the flow in this map. Furthermore, I_∞^+ corresponds to the curves (10) for $z > 0$, while I_∞^- corresponds to the $z < 0$ branch of (10). The curves (10) are singular when $|z| \rightarrow 0$. Because the computation of the Poincaré maps requires the numerical integration of phase space trajectories, we avoid the numerical problems involved with the Coulomb singularity by integrating the trajectories in regularized coordinates (u, P_u, v, P_v) , using the equations of motion (9) arising from \mathcal{K} . In regularized coordinates, the Poincaré map $\rho = 0$ converts to the conditions $u = 0$ and/or $v = 0$ [see Eq. (4)]. Thence, for the sake of completeness, we will also show the corresponding regularized surfaces of section $u = 0$ and $v = 0$.

The evolution of the phase space structure is visualized by computing surfaces of section for $f = -5 \times 10^{-6}$ a.u., for an energy $E = -0.02$ a.u. which corresponds to a principal quantum number $n = 5$, and for some convenient values of the atom–surface distance d ranging in the interval $75a_0 \leq d \leq 300a_0$. Under these conditions, the electron is confined into the infinite potential well because the energy $E = -0.02$ a.u. is below the energy barriers E_{z_p} and E_{z_n} .

When the atom is close to the metal surface, the Poincaré maps in Fig. 4(a) for $d = 75a_0$ show regular behavior. As we can observe in the $u = 0$ and $v = 0$ maps [lower and upper insets in Fig. 4(a)], orbits are ordered forming invariant KAM tori around three central stable fixed points. The central fixed point in the regularized Poincaré maps corresponds to I_∞^- in the $v = 0$ map and to I_∞^+ in the $u = 0$ map. The other two stable fixed points located on the $P_z = 0$ axis are named as C and they correspond to almost circular

orbits travelled in opposite directions. In the regularized Poincaré maps $u = 0$ and $v = 0$ [see the insets of Fig. 4(a)], these periodic orbits C are located at the $P_u = 0$ and $P_v = 0$ axis, respectively. The levels around C are quasiperiodic orbits with the same symmetry patterns as C . In the regularized Poincaré maps a separatrix passing through two unstable fixed points located at the $u = 0$ and $v = 0$ axis separates this new region of motion from the regions of motion around I_∞^- and around I_∞^+ . This is the typical behavior when the interaction of the atom with the metal surface dominates the dynamics [3,7]. Thence, we have three regions of motion populated with orbits with the same symmetry pattern as I_∞^- , I_∞^+ and C , respectively. Examples of each of these kind of quasiperiodic trajectories are shown in Fig. 5.

This structure remains unchanged as the atom moves away from the metal surface (see the surfaces of section in Fig. 4(b) for $d = 125a_0$). However, when $d = 200a_0$ [see Fig. 4(c)], the phase space structure is completely different. Indeed, through two consecutive pitchfork bifurcations (not shown in Fig. 4), the region of motion around C disappears, in such a way that orbits are ordered forming invariant KAM tori around the central stable fixed points I_∞^- and I_∞^+ in the $v = 0$ and in the $u = 0$ Poincaré maps, respectively. In this way, the phase space structure shows a smooth evolution from quasiperiodic orbits around I_∞^- to quasiperiodic orbits around I_∞^+ . Thence, due to the polarizing effect of the field, the system is showing a Stark-like behavior because most of the orbits are oriented along the z direction. When the atom–surface distance is further increased, see Fig. 4(d) for $d = 300a_0$, we find the same phase space structure. It is worth noting that this structure is the classical counterpart of the quantum Stark behavior observed in several studies [1,2] which have revealed that wave functions are strongly oriented along the field direction. The same qualitative behavior was found in [3] for the case $f > 0$.

4. Charge transfer mechanism

In this section we focus on the opposite regime, when the energy is high enough so that the electron can escape from the nucleus attraction. Because for $f < 0$ the ionization of the atom can occur through two different and opposite channels, our objective is to correlate the initial conditions of the electron with the two possible ionization outcomes. To this end, we have calculated the ionization basins of the system trajectories with initial conditions on the Poincaré plane (z, P_z) given by (10). The evolution of the ionization basins has been analyzed for a constant energy $E \approx -3.472 \times 10^{-3}$ a.u. which corresponds to $n = 12$, for a field $f = -5 \times 10^{-6}$ a.u., and for atom–surface distances in the range $100a_0 \leq d \leq 400a_0$. For increasing values of d , the surface barrier raises and the vacuum barrier lowers (see Fig. 2). Thence, we have that up to $d \approx 136a_0$, the only accessible ionization channel for the electron is the negative one; on the contrary, for distances larger than $d \approx 326a_0$ the electron can only escape to the vacuum; and for intermediate distances between the former distances, both the metal and the vacuum ionization channels are simultaneously open. The results of this computation appear in the color maps of Fig. 6, in such way that, red color stands for initial conditions of orbits that are captured by the metal surface (ionization through the negative channel), green color stands for initial conditions of orbits that escape to the vacuum (ionization through the positive channel) and blue color stands for initial conditions of bounded orbits. The insets included in Fig. 6 are the corresponding Poincaré maps $\rho = 0$ with $P_\rho \geq 0$. Based on the same computation of the ionization basins, we have also calculated the ionization probabilities (see Fig. 7).

An overall vision of Fig. 6 shows that the ionization dynamics evolves through three different regimes as the distance d increases. For $d = 100a_0$, the influence of the metal surface dom-

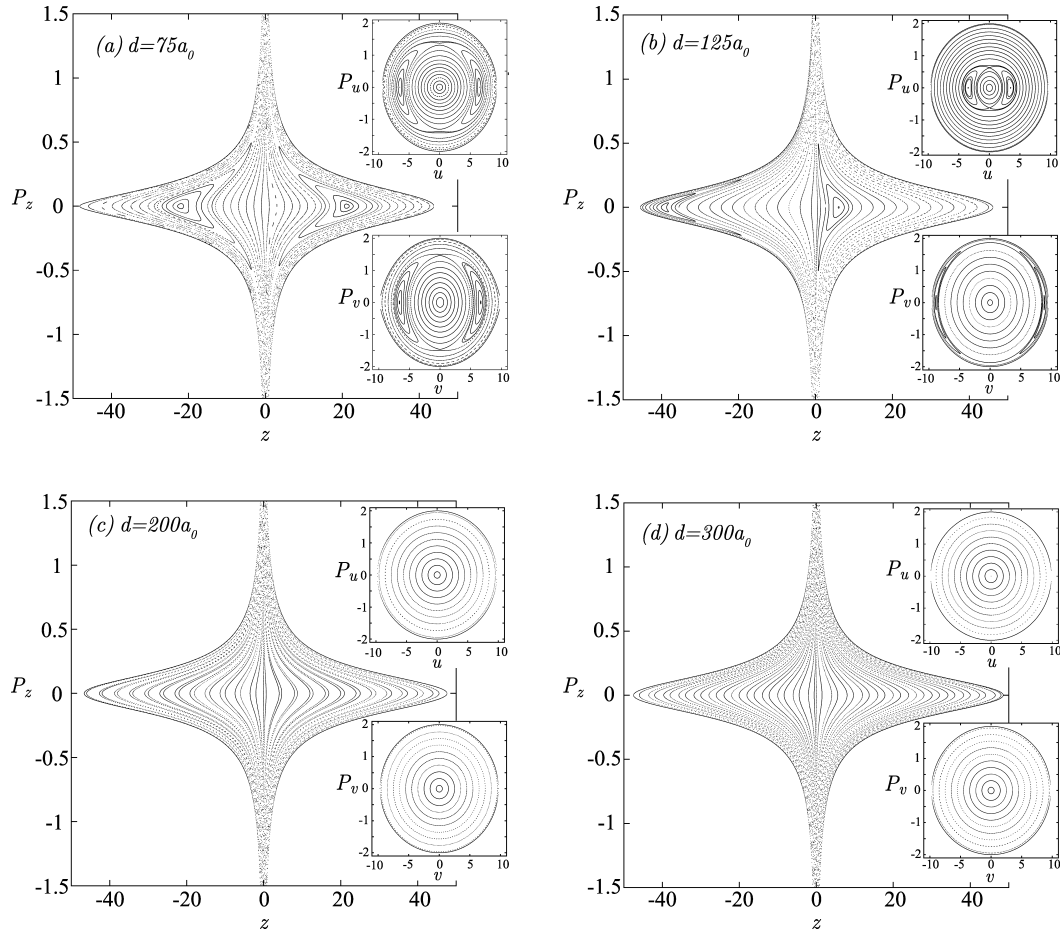


Fig. 4. Poincaré surfaces of section $\rho = 0$ for $d = 75a_0$, $d = 125a_0$, $d = 200a_0$ and $d = 300a_0$. The insets are the corresponding surfaces of section $v = 0$ (upper right corners) and $u = 0$ (lower right corners). All sections for an electric field $f = -5 \times 10^{-6}$ a.u. and for an energy $E = -0.02$ a.u.

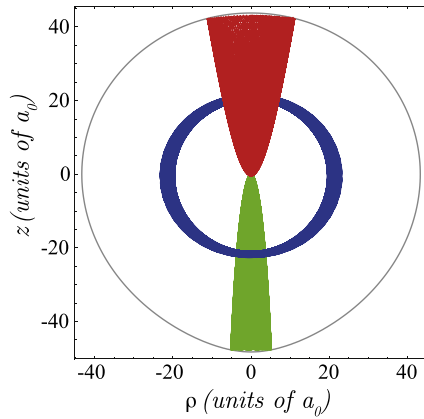


Fig. 5. Quasiperiodic orbits around I_{∞}^{-} (green orbit), I_{∞}^{+} (red orbit) and C (blue orbit). All orbits for $d = 75a_0$, $f = -5 \times 10^{-6}$ a.u. and energy $E = -0.02$ a.u. (For interpretation of the references to color in this figure legend, the reader is referred to the web version of this article.)

inates over the electric field. Hence, in the corresponding color map of Fig. 6(a), the basin of initial conditions of orbits that are captured by the surface coexists with the basin of initial conditions of bounded orbits. Moreover, we observe in Fig. 6(a) that orbits escaping through the surface channel are the rectilinear orbit I_{∞}^{-} and a given portion of the quasiperiodic orbits around it, e.g., those orbits strongly oriented along the surface barrier. These escape orbits create a gap in the corresponding Poincaré section [inset of Fig. 6(a)]. Note that the $z < 0$ side of the Poincaré plane (z, P_z) for $d = 100a_0$ is not bounded because I_{∞}^{-} (the $z < 0$ limit

of the surface of section) is an escape orbit. The phase space region isolated from the surface ionization channel corresponds to I_{∞}^{+} and to the orbits strongly oriented around it. As expected, the evolution of the ionization probabilities in Fig. 7 shows that, for $d < 136a_0$, the ratio between the number of escape orbits through the surface channel and the number of bounded orbits decreases for increasing values of d .

Fig. 6(b) shows the behavior of the system for $d = 200a_0$, when both channels are accessible for ionization, and therefore when three different ionization basins coexist. We note that the ionization basin through the vacuum is located in the phase space region around I_{∞}^{+} . Due to the fact that I_{∞}^{+} is an escape orbit, the $z > 0$ part of the Poincaré plane (z, P_z) is also unbounded. Moreover, for increasing values of d , the metal ionization basin shrinks while the vacuum ionization basin grows in size (see Fig. 6(c) for $d = 300a_0$). As a consequence, the ionization probability through the surface barrier is still decreasing while the ionization probability through the vacuum barrier enhances (see Fig. 7). It is important to note that, even for that high energy value, there always exist sets of initial conditions with a persistent non-ionization behavior.

For atom-surface distances $d > 326a_0$, the effect of the electric field is predominant because only the positive ionization channel is open. Hence, we observe in the color map Fig. 6(d) for $d = 400a_0$ that only the basin of initial conditions of orbits that escape to the vacuum and the basin of initial conditions of non-escape orbits persist. For $d > 326a_0$ the rectilinear orbit I_{∞}^{-} is bounded, so that the $z < 0$ side of the Poincaré plane (z, P_z) in Fig. 6(d) is also bounded.

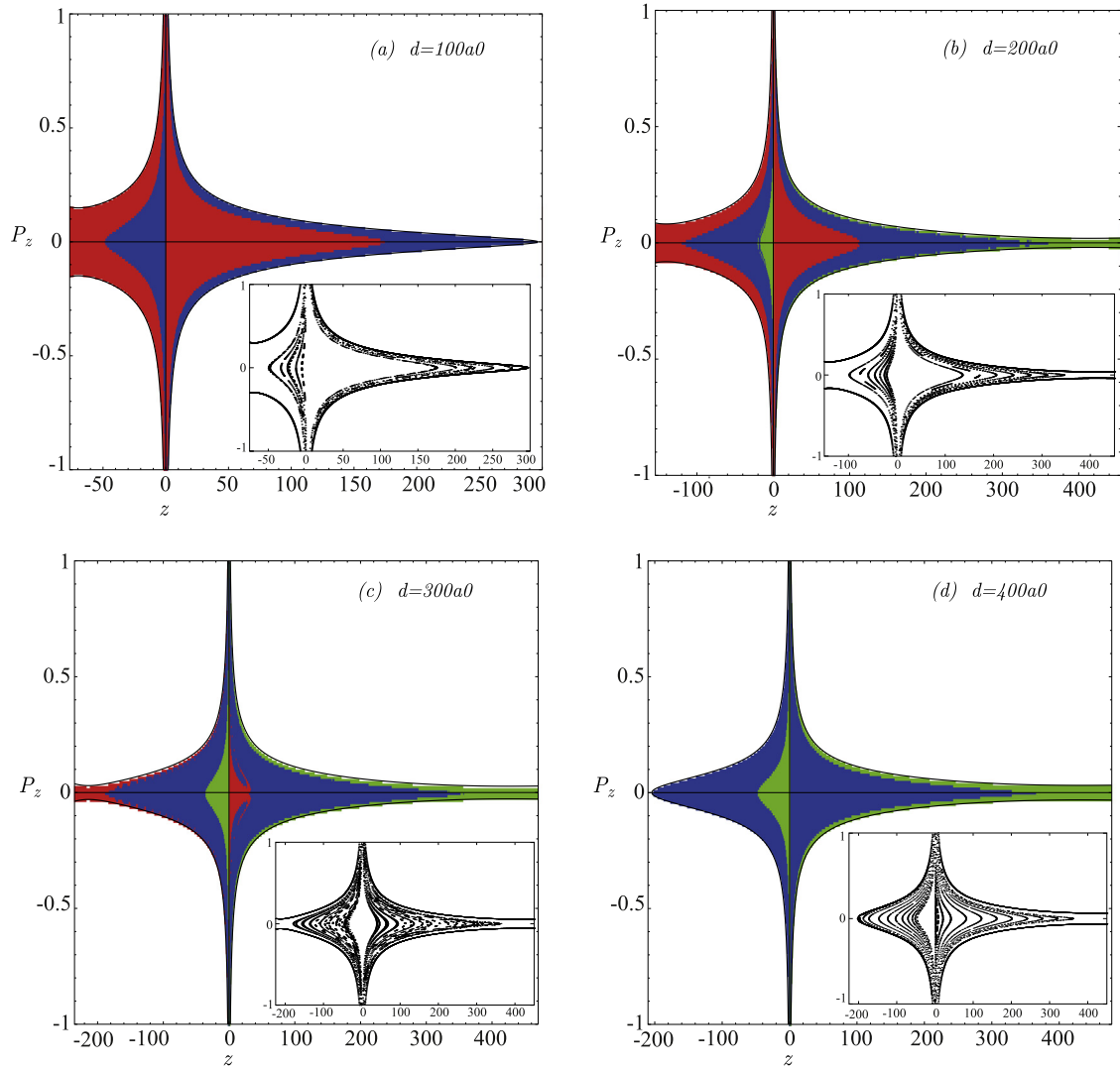


Fig. 6. Evolution of the ionization basins in the $\rho = 0$ planar subspace (z, P_z) for $d = 100a_0$, $d = 200a_0$, $d = 300a_0$ and $d = 400a_0$. The insets are the corresponding surfaces of section $\rho = 0$. All panels for the electric field $f = -5 \times 10^{-6}$ a.u. and for the energy $E \approx -3.472 \times 10^{-3}$ a.u.

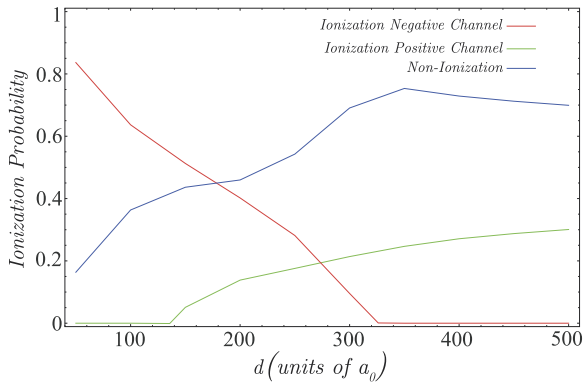


Fig. 7. Evolution of the ionization probabilities as a function of the metal-atom distance d for the electric field value $f = -5 \times 10^{-6}$ a.u. and for the energy $E \approx -3.472 \times 10^{-3}$ a.u.

5. Conclusions

We have studied the classical dynamics of a hydrogen atom near a metallic surface in the presence of a uniform electric field f

in the electron-extraction scheme, e.g., the field is directed to the metal surface ($f < 0$) in such a way that it attracts the electron to the vacuum. To describe the atom-surface interaction we have used a simple electrostatic image model to construct the Hamiltonian of the system. Owing to the axial symmetry of the system, when that Hamiltonian is expressed in cylindrical coordinates, the z component P_ϕ of the angular momentum is conserved, and the system has two degrees of freedom. We have restricted our study to the case $P_\phi = 0$.

By means of Poincaré surfaces of section, we have explored the structure and evolution of the phase space of the system as a function of the negative electric field strength $f < 0$. We have found that, due to the polarizing effect of the field, the system is showing a Stark-like behavior because the electronic orbits are mainly oriented along the z direction. It is worth noting that the dynamical robustness of the rectilinear orbits I_∞^+ and I_∞^- is the responsible for that Stark orientation. Moreover, that classical Stark behavior has its quantum confirmation in several wave packet studies [1,2].

The ionization of the atom has been also investigated by calculating the ionization basins of the system for several surface distances d in the interval $100a_0 \leq d \leq 400a_0$. As the distance d increases in this convenient interval, the ionization of the atom evolves through three different regimes. We empha-

size that the classical results obtained in the study of the charge transfer mechanism are in good agreement with the quantum results of the wave-packet propagation study carried out by So et al. [1] for negative electric field $f < 0$. Indeed, these authors found that quantum states initially oriented towards the vacuum (surface) are likely to ionize at the greatest (smallest) distances.

Acknowledgements

This work has been supported by the research projects MTM2011-28227-C02-01 and MTM2011-28227-C02-02 (Spanish Ministry of Education and Science).

References

- [1] E. So, M.T. Bell, T.P. Softley, *Phys. Rev. A* 79 (2009) 012901.
- [2] J. Hanssen, C.F. Martin, P. Nordlander, *Surf. Sci. Lett.* 423 (1999) L271; Z. Zhou, C. Ourbre, S.B. Hill, P. Nordlander, F.B. Dunning, *Nucl. Instrum. Methods Phys. Res. B* 193 (2002) 403.
- [3] M. Iñarrea, V. Lancharés, J.F. Palacián, A.I. Pascual, J.P. Salas, P. Yanguas, *Phys. Rev. A* 76 (2007) 052903.
- [4] K. Ganesan, K.T. Taylor, *J. Phys. B, At. Mol. Opt. Phys.* 29 (1996) 1293.
- [5] T. Levi-Civita, *Sur la resolution qualitative du problème des trois corps*, vol. 2, University of Bologna Press, Bologna, 1956; E.L. Stiefel, G. Scheifele, *Linear and Regular Celestial Mechanics*, Springer-Verlag, Berlin, 1971.
- [6] M.C. Gutzwiller, *Chaos in Classical and Quantum Mechanics*, Springer-Verlag, Berlin, 1990.
- [7] N.S. Simonovic, *J. Phys. B, At. Mol. Opt. Phys.* 30 (1997) L613.